Position-Sensitive Fast Ionization Chambers

- J. Lai, K. T. Macon, J. C. Blackmon, C. M. Deibel, L. Afanasieva, A. Lauer, L. E. Linhardt, C. Williams
- Department of Physics & Astronomy, Louisiana State University, Baton Rouge, LA 70803

D. Santiago-Gonzalez

- Department of Physics & Astronomy, Louisiana State University, Baton Rouge, LA 70803

 Physics Division, Argonne National Laboratory, Argonne, IL 60439
 - S. Kuvin, J. Belarge, I. Wiedenhover, L. T. Baby, S. Almaraz-Calderon Department of Physics, Florida State University, Tallahassee, FL 32306

E. Need

Department of Physics, Elon University, Elon, NC 27244

B. DiGiovine, C. R. Hoffman, M. L. Avila, B. P. Kay, K. E. Rehm and B. B. Back

Physics Division, Argonne National Laboratory, Argonne, IL 60439

Abstract

A series of high-count-rate ionization chambers have been developed and deployed at several accelerator facilities. Counting rates of ≥ 500 kHz with good Z-separation (up to 5% energy resolution) for particle identification have been demonstrated in a series of commissioning experiments. Additionally, a position-sensitive capability, with a resolution of 3 mm, has been implemented for the first time to record position information and suppress pileup. The design and performance of the detectors are described.

Keywords: Position sensitive, Fast ion chamber

1. Introduction

Measurements of nuclear reactions in inverse kinematics using Radioactive Ion Beams (RIBs) are becoming more prevalent in studies of both nuclear astrophysics and nuclear structure as current accelerators are upgraded and new facilities are developed. However, there are often challenges associated with using RIBs. For example, these beams can be highly contaminated by other species [1] and usually have intensities too low to be measured via conventional means (e.g. a Faraday cup). In addition, the heavy reaction products of interest are often very forward focused. Therefore, detectors that can distinguish between these reaction products, the desired RIB, and contaminants, and can accept rates on the order of RIB intensities (up to $10^5 - 10^6$ pps) are needed for the purpose of measuring beam intensity and composition, as well as detecting heavy reaction products.

Gas ionization detectors or Ionization Chambers (ICs) have been widely utilized for heavy-ion detection since they are robust under intense heavy ion bombardment and provide sound energy resolution with ΔE -E particle identification. Large-scale ionization chambers can be fabricated at relatively low cost, and the effective thickness can also be easily tailored to experimental needs by varying the gas pressure of the detector. However, conventional ionization chambers are limited by slow drift times and pileup becomes problematic at typical RIB intensity ($\leq 10^4$ pps). To improve upon these limitations, Kimura et al. [2] developed a new type of ionization chamber, for high-energy heavy-ion detection at RIKEN, composed of multiple parallel-plane electrodes oriented such that the conductive-foil electrode planes are tilted by 30° relative to the normal of the beam trajectory. Therefore the trajectories of the detected ions pass through the electrode planes instead of running parallel to the electrodes as in more traditional ionization chamber designs [3]. This design has a short and uniform ion drift length that eliminates the position dependence of the signals and improves the timing resolution. As a result, this detector shows significantly improved counting rate ability with reduced pile-up and is proven to be effective in distinguishing particles with different atomic numbers by relative energy loss. A similar design for a fast-counting ionization chamber was adopted by Chae et al. [4] for low-energy nuclear physics measurements, which was constructed and commissioned at Oak Ridge National Laboratory. In this modified design, the

electrode planes were replaced by grids of wires to avoid the additional energy losses that occur when charged particles pass through electrodes planes.

Recently, a series of fast gas ionization chambers were developed at Louisiana State University (LSU), utilizing similar principles as Refs. [2, 4], with the addition of position-sensitivity. This new design was commissioned at the John D.

Fox Accelerator Laboratory at Florida State University (FSU) and the Argonne Tandem LINAC Accelerator System (ATLAS) facility at Argonne National Laboratory. Detectors of this design are also in use at the National Superconducting Cyclotron Laboratory (NSCL). The design, commissioning, and performance of these new detectors is described below.

2. Ionization Chamber Design

The design of these ionization chambers consists of an array of stacked, parallel electrode grids, equally spaced at 2-cm intervals and electrically isolated. Unlike the previous designs of Kimura et al. [2] and Chae et al. [4] that used a tilted electrode design, the grid planes in the LSU design are oriented normal to the beam direction, as shown in Fig. 1. The grids are alternatively grounded cathodes and anodes biased to approximately +250 to +500 V depending on the pressure in the chamber. Based on the specific spatial constraints at each accelerator laboratory, the total number of grids varies from 21 - 27 resulting in an active detector length of 40 - 52 cm (Fig. 1a). The grids used for the cathodes and the non-position sensitive anodes consist of circular aluminum frames with an inner diameter of 17.8 cm and an outer diameter of 21.6 cm (Fig. 1b). Gold-plated tungsten wires of diameter 0.0007" (17.8 μ m), equally spaced at 2-mm intervals, are attached to the frames using conductive epoxy. Unlike the anode planes used by Kimura et al., the wire-grid design allows most low-energy particles to travel through the detector gas without any additional energy loss due to the electrodes; however, there is a small probability that an incoming particle will be intercepted by one of the wires resulting in a loss of efficiency. For grids with 2-mm spaced wires, this loss of efficiency is $\sim 1\%$ per grid. The anodes can be connected internally to create sections with various depths to provide multiple energy loss signals and a measurement of the residual energy, which are read out through BNC feedthroughs. The number of anodes in each section can be adjusted according to the experimental requirements. The cathode grids are all internally connected and then grounded to the body of the chamber (for a more detailed description, see [5]).

A new capability for position sensitivity has been developed for these ionization chambers by replacing a typical anode grid (described above, Fig. 1b) with an anode constructed of electrically isolated wires. In the current design, position-sensitive grids with inner openings of 10 cm x 10 cm were fabricated from G-10 printed circuit boards (Fig. 1c). A total of 32 gold-plated tungsten wires were evenly spaced with 3-mm separation and soldered to VIAs (Vertical Interconnect Access) on opposite sides of the opening. The signal from each wire is read out individually by a multichannel preamplifier. Two of these position-sensitive anode grids are placed at the upstream end of the detector (shown as the second and third anodes in Fig. 1a) and are rotated about the beam axis by 90° relative to each other in order to record both the x and y positions of the incoming particles.

Multiple flanges with aperture sizes up to 6.5" in diameter for the entrance window were fabricated to accommodate reaction studies with a range of recoil ion angles. Depending on the size of the entrance aperture and the gas pressure required in the ionization chamber, both Kapton (poly-oxydiphenylene-pyromellitimide) materials with thicknesses of 7.5 μ m - 25 μ m and Mylar (biaxially-oriented polyethylene terephthalate) materials with thicknesses down to 3 μ m can be used for the window material. Some typical pressures are 50 Torr for a 7.5- μ m Kapton window when the 5"-diameter aperture is used and up to 600 Torr when a 25- μ m Kapton foil is used with the 3.5" aperture. However, high pressure causes stretching of the window, which will lead to additional dead space (of up to 5 cm) upstream of the active volume of the detector, and the distortion is permanent. The addition of a support grid for the window material can reduce this distortion and allow higher pressures, but with an added loss of

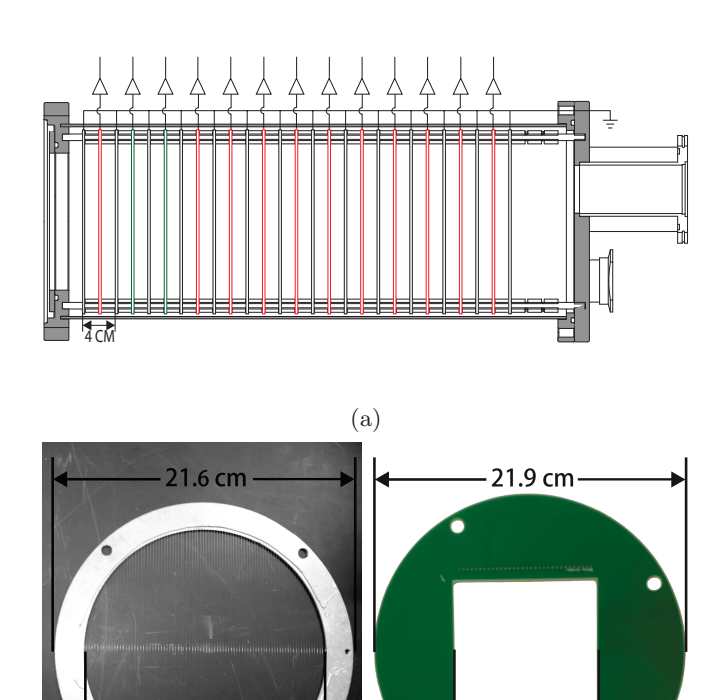


Figure 1: (a) Schematic of the internal grids showing the cathode grids (black), regular anode grids (red), and position-sensitive anode grids (green). Photos of both (b) the regular grids and (c) the position-sensitive grids are also shown.

(b)

10.0 cm

(c)

5 efficiency.

In the original design [2], the tilted electrodes produce an electric field that is not aligned with the beam axis. As a result, the ion-electron pairs are attracted away from beam axis to reduce recombination [6], which increases acceptance of ionized electrons and therefore improves energy resolution. However, in the precense of a strong, axial magnetic field, electrons are bent back to the axis rendering this design ineffective for reducing recombination [5].

A design using non-tilted electrodes is also favored for implementation reasons. For the purpose of detecting recoil ions with lower energies, a thin window foil is typically adopted to minimize particle energy loss. However, such a thin foil will bow out appreciably when the detector is pressurized creating complications in the implementation of the detector and the analysis of resulting data.

Additionally, our simulations show that the non-tilted grid design may improve the resolution from a geometric perspective. Heavy recoils from reactions at low energies may be produced at angles that deviate significantly from 0°. The tilted-grid geometry results in slightly different path distances in the detector for recoils at different ϕ angles, which could degrade the energy resolution. Geant4 simulations of ²⁸Si(¹²C, ¹²C)²⁸Si elastic scattering were performed to study this effect. These simulations reproduced the conditions that exist when the detector is used with a solenoidal magnetic spectrograph, such as the HE-LIcal Orbit Spectrometer (HELIOS) [7]. Microscopic effects are not included in the simulation process. The same properties (e.g. length of ΔE sections, window material and thickness, etc.) are used for both tilted and non-tilted ionization chambers simulations, as shown in Fig. 2 and the distance between the target and IC entrance window was ~ 1 m. The results of these simulations, performed with solenoid field settings of 2.85 T and 0 T, are presented in Fig. 3. The simulated spectra using the tilted-electrode design show observably worse resolution ($\sim 50\%$ worse) compared to the non-tilted simulations. The advantage of using a non-tilted-electrode design becomes even more clear when an axial magnetic field is applied as shown in Fig. 3b. Here the magnetic field refocuses particles emitted at large angles, indirectly increasing angular acceptance of the IC such that heavy ions with the steepest angles are detected. This geometric effect can be further magnified with lower beam energies, lower mass beam particles, a shorter distance between the target and ion detector, etc.

While no experimental data for a direct comparison of the designs is available, the experimental results discussed in the following sections show that this non-tilted grid design has comparable performance.

130

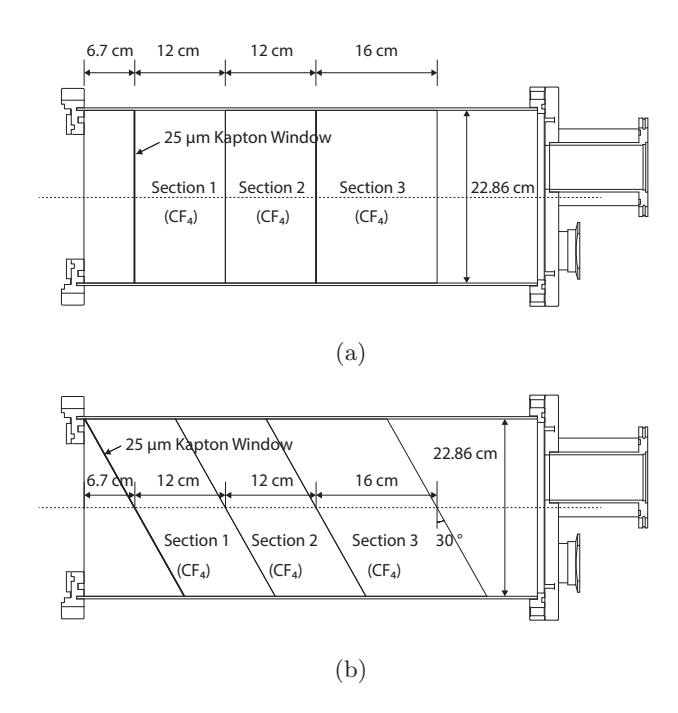


Figure 2: Schematics of the modeled ionization chambers used for simulations with the (a) non-tilted grid design and the (b) tilted grid design. This simulation model consists of a 25 μ m Kapton foil entrance window and three sections of CF₄ gas at 65 Torr.

In general, the signals from the various sections of the fast ionization chambers in all experimental setups were processed by standard NIM electronics, although the specific modules varied depending on availability at each facility. For the data presented here, the ΔE anode signals were first amplified by Canberra preamplifiers. The output signals from the preamplifiers were then fed into fast spectroscopy amplifiers for further processing. We find that two-bin-

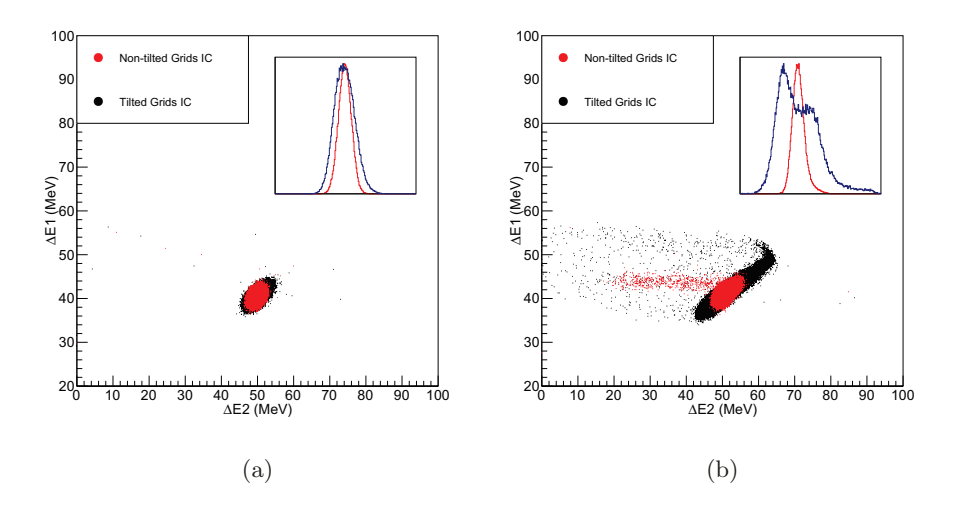


Figure 3: Results from Geant4 simulations of detector performance comparing data from the non-tilted-grid IC (red) with data from the tilted-grid IC (black) with (a) no magnetic field applied and (b) measured field map from HELIOS applied. Projections of the spectra along the X axes are plotted in the insets, where the data are normalized to each other.

size Canberra (model 2024) and Tennelec (TC 203BLR) amplifiers have good performance at high counting rates. Signals from the position-sensitive grids are amplified using a customized multichannel preamplifier box and further shaped through a MesyTec amplifier (MSCF-16-F). It should be noted that the MesyTec amplifier cannot handle rates above 100 kHz, and the overall counting rate reflected in the position-sensitive ΔE sections are split over 32 channels.

5 3. Results

3.1. Ionization Chamber Spectra and Resolution

Commissioning data for the ionization chamber was taken at the ATLAS facility using the HELIcal Orbit Spectrometer (HELIOS) [7] beam line with a 6-MeV/A 28 Si beam impinging upon a natural C target. HELIOS is a large magnetic solenoid, which has a strong residual magnetic field at the location of the IC. Unless otherwise specified, the magnetic field of HELIOS was set to 2.85 T resulting in a fringe field of ~ 0.5 T at the location of the IC. The anodes

inside the IC were grouped into three sections with three, three, and four anodes sequentially comprising each of these sections. The position-sensitive grids were not installed during these initial tests at ATLAS.

Figure 4 shows a typical spectrum of the energy loss in the first IC section ($\Delta E1$) as a function of the energy loss in the second section ($\Delta E2$). A 1-cm diameter blocker was placed at 0° to block the incident ²⁸Si beam. The most intense component in the spectra is from the scattered ²⁸Si beam. In addition to the scattered beam group, a series of particle groups with constant $\Delta E1$ values are observed, which are due to the interception of incoming particles by the tungsten wires of the grids in the $\Delta E2$ section. Similarly, a series of particle groups at $\Delta E2 = 0$ are observed when particles stop within the $\Delta E1$ section.

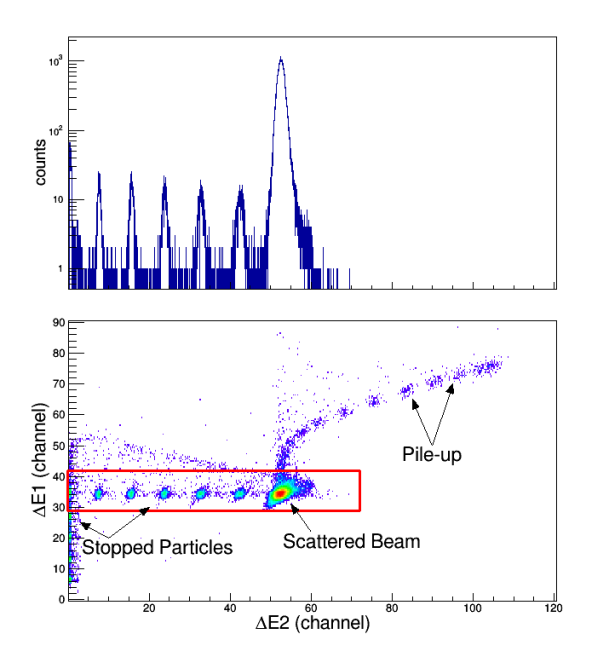


Figure 4: In the lower plot a typical spectrum of energy loss in the first IC section (Δ E1) vs. the second IC section (Δ E2) from elastic scattering of a ²⁸Si beam on a natural carbon target is shown. The main particle group from the scattered beam, as well as the groups from pileup and particles stopped by the detector grids, are labeled for clarity. The data inside the red box are projected along the x axis in the upper plot.

The ²⁸Si beam produced from the ATLAS facility is bunched at 82-ns intervals. Discrete timing separation between beam pulses results in quantized amplitudes for pileup signals as shown in Fig. 4. By contrast, in the case of a direct-current beam, a continuous pileup band would be observed. This pileup can be suppressed using data from the position-sensitive grids as discussed in Section 3.2.

The dependency of energy resolution on the bias voltage of the anodes and counting rate was examined using $^{28}\mathrm{Si}(^{12}\mathrm{C},^{12}\mathrm{C})^{28}\mathrm{Si}$ scattering. As the IC is located in a strong fringe field that can potentially affect electron drifting trajectories, the resolution was also studied both with and without the magnetic field applied. For the purpose of measuring the intrinsic resolution of the detector system, the gas pressure inside the IC was intentionally chosen to enable the heavy recoils to be detected in three sections: two $\Delta \mathrm{E}$ sections and a residual energy section. Due to straggling in the target, IC window, and IC gas, the residual energy detected in the last active section of the IC typically has the worst resolution. Therefore, only signals from the first two $\Delta \mathrm{E}$ sections will be used for the characterization of detector resolution.

After calibration, 1D spectra for $\Delta E1$ and $\Delta E2$ are fitted by a skew-normal distribution and the full width half maximum (FWHM) is calculated. Uncertainties shown in Figs. 5, 6 and 7 (90% CI) are obtained using the bootstrap method [8].

Figure 5 shows the resolution in the second section of the IC (Δ E2) as a function of counting rate, under a 2.85-T magnetic field in HELIOS. The detector was filled with 65 Torr isobutane gas and biased at +225 V. The resolution deteriorates as counting rate increases and the effect of pileup becomes significant (\geq 12%) for rates above 150 kHz. This trend is also observed in the resolution vs. counting rate plot of section 1 (Δ E1), also shown in Fig. 5.

To illustrate the effect of anode bias on resolution, data taken with anode biases ranging from +150 V to +500 V are compared with the +225 V data set in Fig. 6. This figure shows that lower bias is associated with worse resolution, especially at high counting rates, likely due to slow collection times and

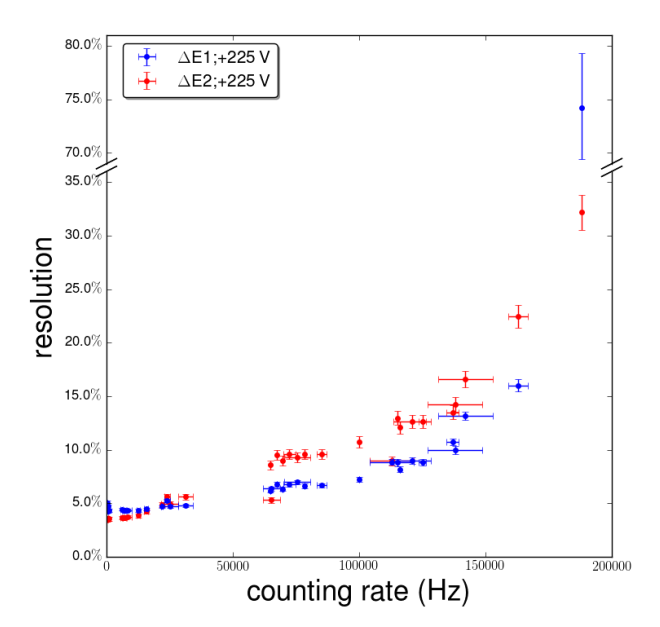


Figure 5: (Color online) Plot of resolution vs. counting rate with the detector anodes biased to +225 V. The resolution of the first ($\Delta E1$) and second ($\Delta E2$) sections of the detector are plotted in blue and red, respectively.

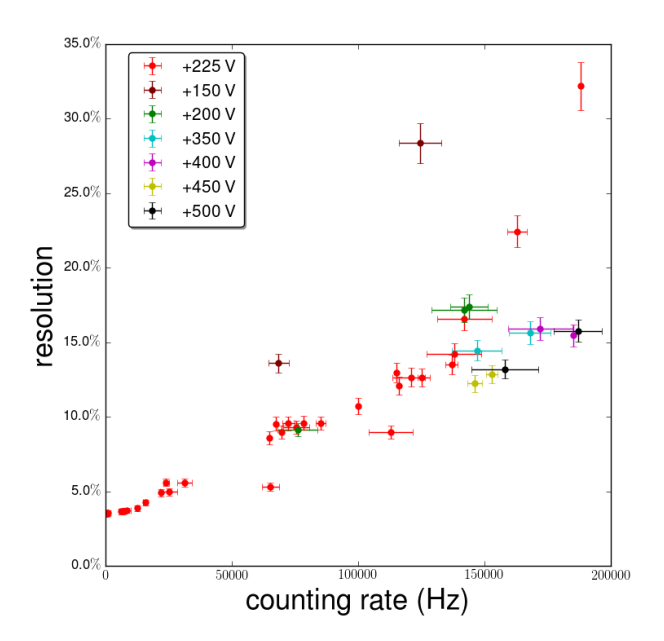


Figure 6: (Color online) Plot of resolution as a function of counting rate for the second section of the detector (Δ E2). Voltages for different data sets are given in the legend.

recombination effects.

Figure 7 shows a detailed study of magnetic field effects on detector resolution as a function of counting rate. A blocker is installed in front of the IC to shield particles at 0°. In addition, the data shown in Fig. 7 were taken using the IC filled with 65 Torr of CF₄ gas and biased to +500 V. Improved energy resolution is observed in Fig. 7 compared to Figs. 5 and 6, and is most likely due to a combination of factors, including gas type, bias, and reduced recombination effects resulting from a smaller intensity per detector volume of the scattered particles compared with the direct beam when the blocker is not in use. Measurements with the maximum magnetic field of HELIOS (2.85 T) applied consistently yield better resolution than those with no magnetic field. This improvement in resolution is more pronounced with higher counting rates.

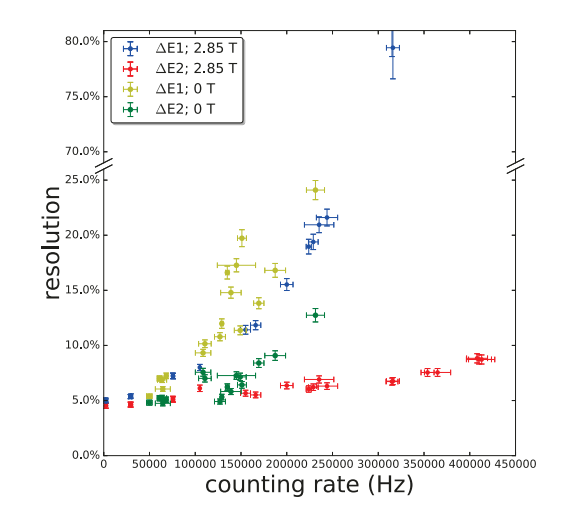


Figure 7: Resolution in sections one and two of the IC as a function of counting rate for 0 T and 2.85 T magnetic field in HELIOS.

While 1D spectra have been used here to quantitatively show correlations between resolution and some parameters (counting rates, high voltage bias, and magnetic field), the ionization chamber's abilities to separate different particle groups are better realized when data are presented in two dimensional plots,

such as $\Delta E1$ vs $\Delta E2$ (e.g. Fig. 4). For example, the ionization chamber was used in a recent measurement of the $^{20}\mathrm{Ne}(\alpha,p)^{23}\mathrm{Na}$ and $^{20}\mathrm{Ne}(d,p)^{21}\mathrm{Ne}$ reactions in inverse kinematics where the detector was consistently run at counting rates higher than 400 kHz, while maintaining resolution sufficient for separating particle groups of $^{20}\mathrm{Ne}$, $^{21}\mathrm{Ne}$, and $^{23}\mathrm{Na}$ [9] in 2D histograms, which could not be distinguished in a 1D ΔE spectrum.

Though no systematic Z resolution test was performed, the ability of these ionization chambers to separate particle groups based on Z has been tested under a variety of conditions. As an example of particle identification, a spectrum from a ³⁰S beam production experiment is presented in Fig. 8. The IC was operated under 4.5-kHz counting rate and filled with 300 Torr of CF₄ gas. The ³⁰S beam was produced via the ²⁸Si(³He,n)³⁰S reaction by bombarding a ³He gas target with a stable, 325-MeV ²⁸Si beam. The spectrum shows that ³⁰S is well separated from other components, with a Z-resolution of 0.22 between ²⁸Si and ²⁹P.

3.2. Position Sensitive Grids

225

As discussed in Sec. 2, a new position-sensitive capability was implemented for these ionization chambers. The data presented in this section are from experiments performed at FSU using an annular Si strip detector, segmented in both θ and ϕ angles. The Si detector is located downstream of the target, followed by the ionization chamber, as shown in Fig. 9. The position-sensitive grids were initially tested using data from $^{1}\text{H}(^{17}\text{O},^{1}\text{H})^{17}\text{O}$ proton elastic scattering and the $^{1}\text{H}(^{17}\text{O},^{4}\text{He})^{14}\text{N}$ reaction. By selecting events in coincidence between the Si detector and IC, we are able to study correlations between the light and heavy recoils. Figure 10a shows a strong correlation between the ϕ -angle from the position-sensitive grids and the ϕ -angle detected by the silicon detector from $^{17}\text{O}+p$ scattering data. The spectrum shown in Fig. 10b gives the position distribution of data events from both the (p,α) reaction and (p,p) scattering on an ^{17}O beam and a clear spatial separation is observed between recoils of ^{17}O and ^{14}N . This angular and position information can be used to identify the light

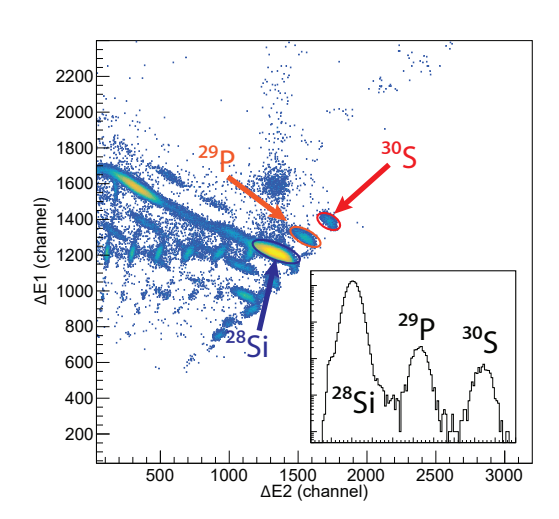


Figure 8: Spectrum of $\Delta E1$ vs $\Delta E2$ for the ^{30}S radioactive ion beam production test at ATLAS. Particle groups corresponding to the desired ^{30}S beam, the stable, primary ^{28}Si beam, and the ^{29}P contaminant beam are labeled and clearly separated. Other "particle" groups are due to beam particles that are stopped by the wire grids, different charge states and/or contaminants produced via the $^{28}Si+^{3}He$ reaction channel. A Z-resolution histogram of ^{28}Si , ^{29}P , and ^{30}S is plotted in the inset.

an ad

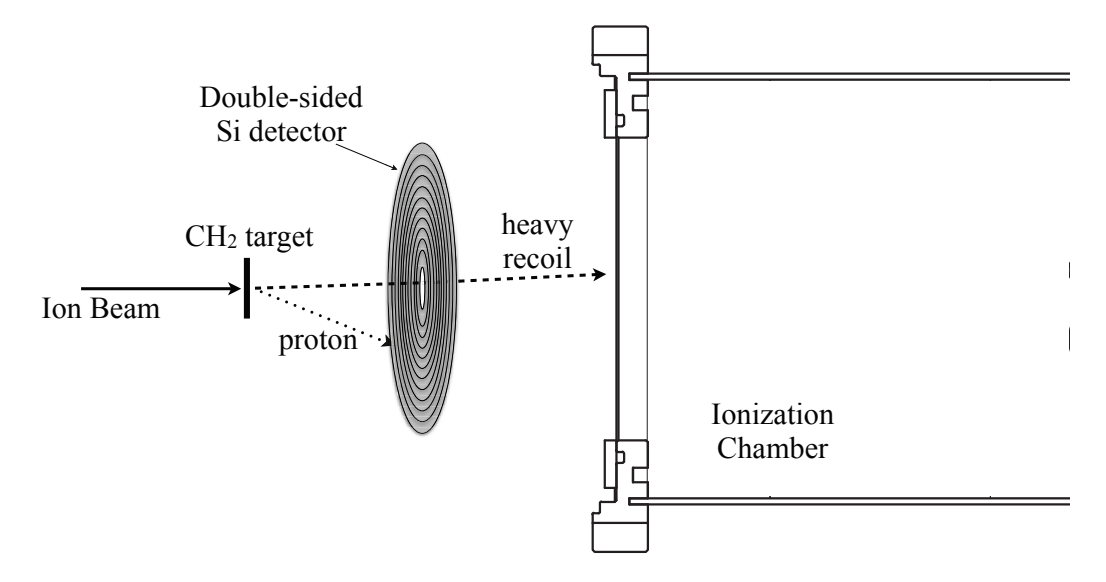


Figure 9: Schematic (not to scale) of the experimental setup at Florida State University for the commissioning of the position-sensitive capability of the ionization chambers.

Such angular information was recently utilized in a series of (d, n) reaction measurements ($^{25}\text{Al}(d, n)^{26}\text{Si}$ [10], $^{17}\text{F}(d, n)^{18}\text{Ne}$ [11] and $^{19}\text{Ne}(d, n)^{20}\text{Na}$ [12]) studying states corresponding to resonances of interest populated via proton-capture reactions. For states above the proton separation energy, the neutrons need not be detected, but can be reconstructed from the angles and energies of the emitted protons. Previously, the neutron energy reconstruction was based on the assumption that primary reactions are aligned with the beam axis [13]. This assumption is removed by using the θ angles of the recoils from the position sensitive grids and the resolution of the obtained resonance energy is significantly improved (Fig. 11).

Additionally, these position-sensitive grids can also be used for suppressing pileup. If two particles enter the chamber with a spatial separation larger than ~ 3 mm in the XY plane, the position-sensitive grids can give information on multiplicity, independent of the time separation between events. Figure 12 shows

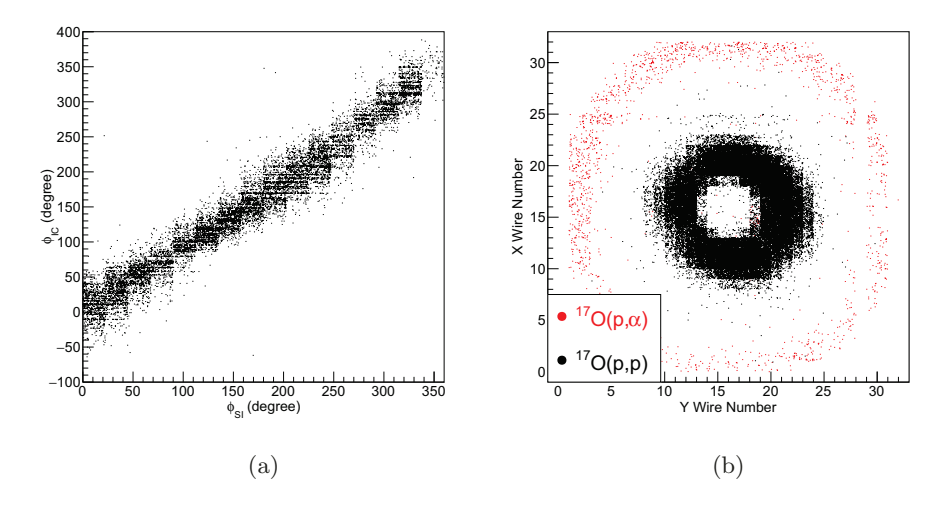


Figure 10: (a) Azimuthal angle of protons detected in the DSSD vs ϕ angle of recoils as measured by the IC from $^{1}\text{H}(^{17}\text{O},^{1}\text{H})^{17}\text{O}$ scattering; (b) x and y position (plotted as the wire number of the X and Y grids) from $^{1}\text{H}(^{17}\text{O},^{1}\text{H})^{17}\text{O}$ scattering (black) and the $^{1}\text{H}(^{17}\text{O},^{4}\text{He})^{14}\text{N}$ reaction (red).

that, in the study of ${}^{2}\mathrm{H}({}^{17}\mathrm{F},n){}^{18}\mathrm{Ne}^*(p){}^{17}\mathrm{F}$, the pileup is reduced by requiring a multiplicity of one in the position-sensitive grid data.

4. Summary

260

Gas ionization chambers with wire grids normal to the beam axis have been designed at LSU and commissioned at ANL and FSU to fit the needs of complicated experimental environments. The chambers can work stably at beam intensities up to at least 500 kHz with reasonable resolution, though the resolution does degrade as the counting rate increases. A position-sensitive capability has been developed and implemented for the first time in order to acquire position and angular information, which can also be used for pileup suppression. These detectors are now in use at a variety of accelerator facilities at ANL, FSU and Michigan State University and have been used in multiple transfer and direct reaction measurements [9, 14].

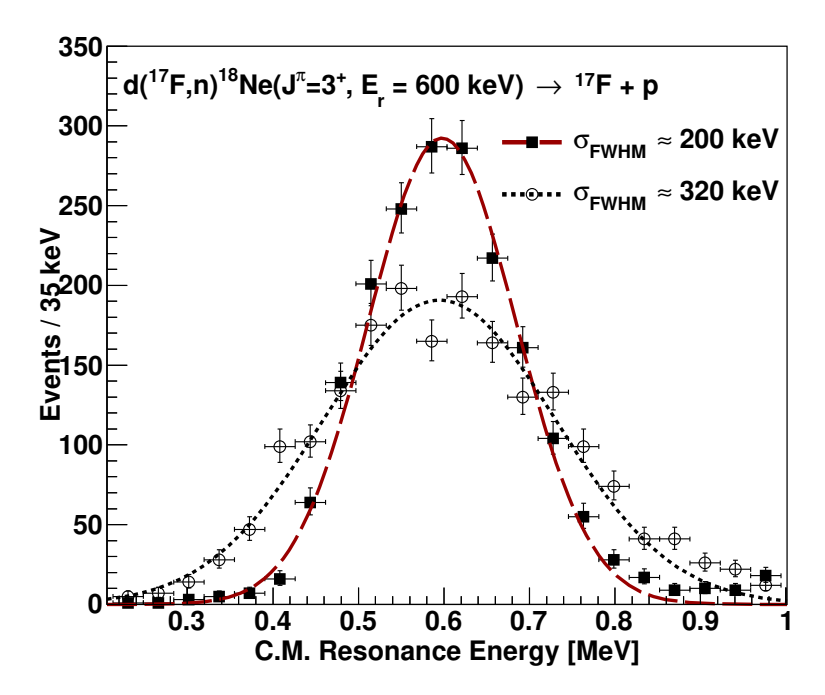


Figure 11: Reconstruction of resonance energy of the 600-keV, 3^{+} ¹⁸Ne resonance populated via $d(^{17}F,n)^{18}Ne^*(p)^{17}F$ with (long dashed red line) and without (short dashed black line) heavy recoil angular information.

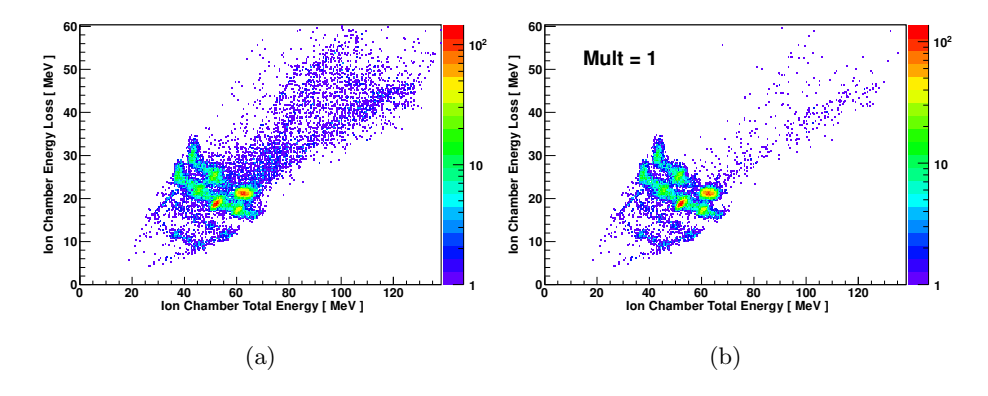


Figure 12: Energy loss vs total energy in the ionization chamber for 17 F particles from the 2 H(17 F,n) 18 Ne*(p) 17 F reaction (a) without and (b) with a multiplicity condition on the position sensitive grids applied. A clear decrease in pileup is seen when the condition that multiplicity equals 1 is applied.

270 5. Acknowledgements

This work was partially supported by the U.S. Department of Energy, Office of Science, Office of Nuclear Physics under contract numbers DE-FG02-96ER40978 and DE-AC02-06CH11357, Louisiana Board of Regents RCS Subprogram Contract LEQSF(2012-15)-RD-A-07, and FSU Grant ##. This research used resources of ANL's ATLAS facility, which is a DOE Office of Science User Facility.

References

280

285

290

295

- B. Harss, R. Pardo, K. Rehm, F. Borasi, J. Greene, R. Janssens, C. Jiang, J. Nolen, M. Paul, J. Schiffer, et al., Review of Scientific Instruments 71 (2000) 380.
- [2] K. Kimura, T. Izumikawa, R. Koyama, T. Ohnishi, T. Ohtsubo, A. Ozawa, W. Shinozaki, T. Suzuki, M. Takahashi, I. Tanihata, et al., High-rate particle identification of high-energy heavy ions using a tilted electrode gas ionization chamber, Nuclear Instruments and Methods in Physics Research Section A: Accelerators, Spectrometers, Detectors and Associated Equipment 538 (1) (2005) 608–614.
- [3] G. F. Knoll, Radiation Detection and Measurement, 3^{rd} ed., New York, Wiley, 1999.
- [4] K. Chae, S. Ahn, D. Bardayan, K. Chipps, B. Manning, S. Pain, W. Peters, K. Schmitt, M. Smith, S. Strauss, Nuclear Instruments and Methods in Physics Research Section A 751 (2014) 6.
 - [5] J. Lai, A DIRECT STUDY OF THE 20Ne (α, p) 23Na REACTION WITH THE HELICAL ORBIT SPECTROMETER (HELIOS), Ph.D. thesis, Faculty of the Louisiana State University and Agricultural and Mechanical College in partial fulfillment of the requirements for the degree of Doctor of Philosophy in The Department of Physics and Astronomy by Jianping Lai BS, Huazhong University of Science and Technology (2016).

- [6] W. C. Sailor, S. G. Prussin, Nuclear Instruments and Methods in Physics Research Section A 274 (1989) 305.
- [7] J. Lighthall, B. Back, S. Baker, S. Freeman, H. Lee, B. Kay, S. Marley, K. Rehm, J. Rohrer, J. Schiffer, et al., Nuclear Instruments and Methods in Physics Research Section A 622 (2010) 97.
 - [8] B. Efron, R. J. Tibshirani, An introduction to the bootstrap, CRC press, 1994.
- ³⁰⁵ [9] J. Lai, et al., A direct study of 20 Ne $(\alpha,p)^{23}$ Na reaction with the HELIcal Orbit Spectrometer (HELIOS), in preparation (2016).
 - [10] J. Baker, Measurement of the 25 Al $(d, n)^{26}$ Si Reaction at RESOLUT, Ph.D. thesis, Florida State University (2015).
- [11] S. Kuvin, Measurement of the 16 F $(d,n)^{18}$ Ne Reaction at RESOLUT, Ph.D. thesis, Florida State University (2015).
 - [12] J. Belarge, S. Kuvin, L. Baby, J. Baker, I. Wiedenhöver, P. Höflich, A. Volya, J. Blackmon, C. Deibel, H. Gardiner, et al., Experimental Investigation of the 19 Ne(p, γ) 20 Na Reaction Rate and Implications for Breakout from the Hot CNO Cycle, Physical review letters 117 (18) (2016) 182701.
- [13] P. Peplowski, L. Baby, I. Wiedenhöver, S. Dekat, E. Diffenderfer, D. Gay, O. Grubor-Urosevic, P. Höflich, R. Kaye, N. Keeley, et al., The lowest L = 0 proton resonance in silicon-26 and its implications for the stellar nucleosynthesis of aluminum-26, Physical Review C 79 (3) (2009) 032801.
 - [14] A. Lauer, et al., in preparation (2016).